Structural Studies of Langerin and Birbeck Granule: A Macromolecular Organization Model[†,‡]

Michel Thépaut,[§,||,⊥,#] Jenny Valladeau,[§,▽] Alessandra Nurisso,[○] Richard Kahn,[||,⊥,#] Bertrand Arnou,[||,⊥,#,○] Corinne Vivès,[||,⊥,#] Sem Saeland,[◇] Christine Ebel,[⊥,#,△] Carine Monnier,[||,⊥,#] Colette Dezutter-Dambuyant,[▽] Anne Imberty,[○] and Franck Fieschi*[,||,⊥,#]

Laboratoire des Protéines Membranaires and Laboratoire de Biophysique Moléculaire, CEA, DSV, Institut de Biologie Structurale (IBS), 41 rue Jules Horowitz, Grenoble F-38027, France, CNRS, UMR 5075, Grenoble, France, Université Joseph Fourier, Grenoble F-38000, France, Centre Léon Bérard, INSERM U590, Lyon, France, CERMAV-CNRS, Grenoble, France, and DermImmune, 6 rue Sœur Bouvier, 69005 Lyon, France

Received November 21, 2008; Revised Manuscript Received January 28, 2009

ABSTRACT: Dendritic cells, a sentinel immunity cell lineage, include different cell subsets that express various C-type lectins. For example, epidermal Langerhans cells express langerin, and some dermal dendritic cells express DC-SIGN. Langerin is a crucial component of Birbeck granules, the Langerhans cell hallmark organelle, and may have a preventive role toward HIV, by its internalization into Birbeck granules. Since langerin carbohydrate recognition domain (CRD) is crucial for HIV interaction and Birbeck granule formation, we produced the CRD of human langerin and solved its structure at 1.5 Å resolution. On this basis gp120 high-mannose oligosaccharide binding has been evaluated by molecular modeling. Hydrodynamic studies reveal a very elongated shape of recombinant langerin extracellular domain (ECD). A molecular model of the langerin ECD, integrating the CRD structure, has been generated and validated by comparison with hydrodynamic parameters. In parallel, Langerhans cells were isolated from human skin. From their analysis by electron microscopy and the langerin ECD model, an ultrastructural organization is proposed for Birbeck granules. To delineate the role of the different langerin domains in Birbeck granule formation, we generated truncated and mutated langerin constructs. After transfection into a fibroblastic cell line, we highlighted, in accordance with our model, the role of the CRD in the membrane zipping occurring in BG formation as well as some contribution of the cytoplasmic domain. Finally, we have shown that langerin ECD triggering with a specific mAb promotes global rearrangements of LC morphology. Our results open the way to the definition of a new membrane deformation mechanism.

Dendritic cells (DCs)[1] are professional antigen-presenting cells able to specifically stimulate naive T-cells. They are in an immature state in mucosal and peripheral tissues. During migration to lymph nodes, they undergo a maturation process ending by the presentation of processed antigens to naive T lymphocytes (*1*). DCs can be divided into several subsets distinguishable by the expression of specific C-type lectins. Indeed, Langerhans cells (LCs), and a small subset of dermal DCs, specifically express langerin (CD207) (*2*) while other mucosal DCs express DC-SIGN (CD209) that has been subject to intense studies since its role in HIV transmission has been highlighted (*3*).

LCs are characterized by the presence of Birbeck granules (BG), pentalamellar and zippered membranes defining rod-shaped structures of different sizes with a central, periodically striated lamella (*4*). The correlation between langerin ac-

[†] Financial support from B. & M. Gates Foundation for M.T. postdoctoral grant and EEC Marie-Curie MEST-CT-2004-503322 training program for partial financing of A.N. "Sidaction-Ensemble contre le Sida" is also acknowledged for its financial support during the initial stages of this work.

[‡] Langerin CRD coordinates and structure factors have been deposited in the Protein Data Bank, ID code 3C22.

* Corresponding author. E-mail: fieschi@ibs.fr. Tel: +33-(0)-4-38-78-91-77. Fax: +33-(0)-4-38-78-54-94.

[§] These two authors have equally contributed to the work.

[||] Laboratoire des Protéines Membranaires, CEA, DSV.

[⊥] CNRS, UMR 5075.

[#] Université Joseph Fourier.

[▽] Centre Léon Bérard.

[○] CERMAV-CNRS.

[◇] DermImmune.

[△] Laboratoire de Biophysique Moléculaire, CEA, DSV.

[1] Abbreviations: αMan12Man, α-D-mannose-(1−2)-α-D-mannose; BG, Birbeck granules; BSA, bovine serum albumin; bp, base pairs; *c*(*s*), continuous distribution; CMS, cytomembrane sandwiching structures; CRD, carbohydrate recognition domain; DC, dendritic cells; DC-SIGN, dendritic cell-specific ICAM-3-grabbing non-integrin; DC-SIGNR, dendritic cell-specific ICAM-3-grabbing non-integrin-related protein; DLMM, double labeling minimum medium; ECD, extracellular domain; EDTA, ethylenediaminetetraacetic acid; ESRF, European Synchrotron Radiation Facility; HBSS, Hank's buffered salt solution; HIV, human immunodeficiency virus; IPTG, isopropyl β-D-1-thiogalactopyranoside; LC, Langerhans cells; Lg, langerin; M12M, α-D-mannose-(1−2)-α-methyl-D-mannoside; M12M12M, α-D-mannose-(1−2)-α-D-mannose-(1−2)-α-methyl-D-mannoside; M12M13M, α-D-mannose-(1−2)-α-D-mannose-(1−3)-α-methyl-D-mannoside; mAb, monoclonal antibody; MBP, mannose-binding protein; MIRAS, multiple isomorphous replacement with anomalous scattering; R_S, Stokes radius; $s_{20,w}$, corrected sedimentation coefficient at 20 °C in water; S-CRD, strep-tagged carbohydrate recognition domain; SDS−PAGE, sodium dodecyl sulfate−polyacrylamide gel electrophoresis; ΔCyto, deletion of the cytoplasmic domain (amino acids 1 to 28); ΔCRD, deletion of the carbohydrate recognition (amino acids 189 to 328); P231, point mutation of Pro23 into Ile.

10.1021/bi802151w CCC: $40.75
Published on Web 01/28/2009

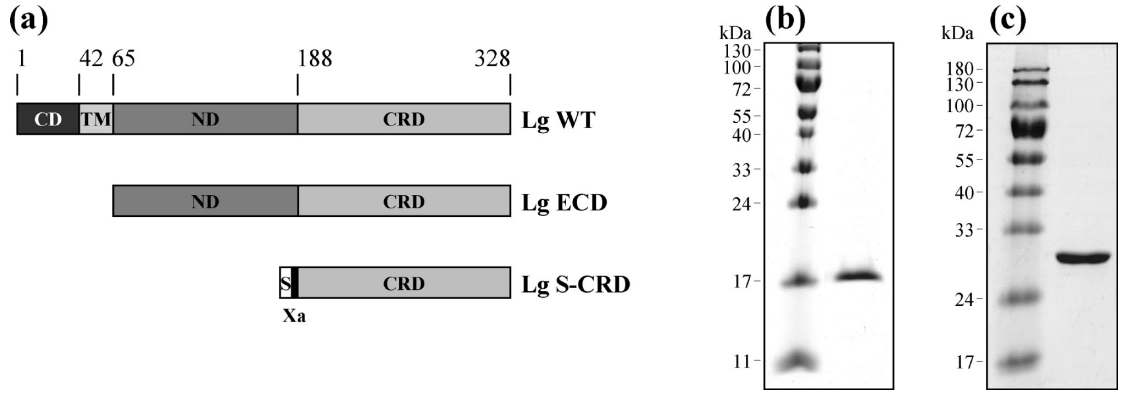

FIGURE 1: Langerin constructs used in these studies. (a) Representations of langerin domain organization and constructs used in these studies. CD, cytoplasmic domain; TM, transmembrane region; ND, neck domain required for oligomerization; CRD, carbohydrate recognition domain. For the Lg S-CRD construct a strep-tag II affinity tag was added to the N-terminus (noted S), followed by a Xa factor proteolytic site. (b, c) SDS−PAGE homogeneity analysis after purification of Lg S-CRD and Lg ECD, respectively.

cumulation and BG formation has been clearly demonstrated by the induction of their formation into fibroblasts or melanoma cell lines transfected with langerin cDNA (*2, 5*). Langerin is a type II membrane protein with an extracellular domain (ECD) containing a neck region and a C-type carbohydrate recognition domain (CRD) (*2, 6*). Its Ca^{2+}-dependent lectin properties have been confirmed (*7, 8*) with a monosaccharide specificity for mannose, fucose, and *N*-acetylglucosamine (*9*).

The roles of Birbeck granules are still a matter of debate. A disruption of the langerin gene in a mouse model did not induce any marked phenotypic alteration, apart from the disappearance of BGs. Indeed, no difference was observed compared to normal mice, in development, LC number in epidermis, antigen capture, nor LC maturation (*10*). Nevertheless, as illustrated for *Mycobacterium leprae* (*11*), a specific mobilization of langerin, in conjunction with CD1a, was demonstrated in the efficient presentation of nonpeptide antigen to T-cells. LCs, as other DCs, have been reported to bind HIV-1 and were then assumed to transmit HIV-1 to T-cells via langerin similarly to DC-SIGN (*12*). Moreover, LCs are localized in mucosal epithelia, and thus, during the initial exposition to HIV-1, they are the first DC subset in contact with the virus, emphasizing the potential importance of this DC subset in HIV infection (*13*). Recently, De Witte et al. brought new elements, criticized this point of view, and showed that langerin was able to inhibit LC infection and prevent HIV-1 transmission (*14*). They showed that HIV-1 is captured by langerin internalized into BGs and suggest its subsequent degradation. Therefore, langerin CRD may be directly involved in two phenomena: HIV-1 binding and Birbeck granule formation.

A better understanding of the interaction of langerin with HIV-1 as well as the involvement of this lectin in BG architecture requires detailed biochemical and structural characterization. Moreover, such studies are necessary to define a molecular strategy to selectively inhibit DC-SIGN without affecting langerin. The two lectins are most similar in their CRD domain while strong divergence, inducing different oligomerization states, exists in their neck domain. We have produced the CRD domain and the whole ECD of human langerin and solved the CRD structure at 1.5 Å resolution. A lower resolution structure of a slightly shorter version of langerin CRD, complexed with mannose and maltose, was very recently published (*15*). On the basis of our structure, gp120 N-glycan oligosaccharide binding was predicted by molecular modeling and compared with the published structure of the carbohydrate/CRD complexes mentioned above. Moreover, we report hydrodynamic studies on the purified langerin ECD. Resulting parameters were used to support a molecular model of the trimeric langerin ECD integrating the X-ray structure of the CRD. In parallel, electron microscopy analysis of BGs from isolated Langerhans cells is reported. From the dimension observed and the generated molecular model of the langerin ECD, a supramolecular organization of the BG is proposed. We have used different modified langerin constructs transfected in fibroblastic cells to determine the relative importance of the various domains of langerin in BG formation. Finally, we have shown that triggering of langerin ECD with specific mAb induces global rearrangements of LC morphology, which define of a novel membrane deformation mechanism.

EXPERIMENTAL PROCEDURES

Cloning and Expression of Recombinant Langerin Domains. Lg S-CRD (Figure 1) was expressed as previously described (*16*). The expression protocol of the Se-labeled Lg S-CRD used to solve the structure required a slightly different cloning. The cDNA coding for the Lg S-CRD was transferred into pET-15b vector (Novagen) since an ampicillin resistance vector was required for the production of Se-labeled Lg S-CRD. This latter plasmid was sequence checked and used to transform calcium-competent auxotrophic *Escherichia coli* BL21(DE3) selB::kan cys51E cells ($BL21_{cys}$) (*17*). Se-labeled Lg S-CRD was expressed using SeMet/SeCys double labeling (*18*). The pellet obtained from a 150 mL overnight culture was used to inoculate a 3 L culture in DLMM. The culture was grown at 37 °C for 6 h, and expression was induced by 1 mM IPTG. After 15 min incubation the cells collected by centrifugation were resuspended in 3 L of DLMM completed with 1 mM IPTG, 600 μM L-Se-cystine, and 425 μM L-Se-methionine. About 13 g of cells was collected after overnight incubation at 25 °C.

Lg-ECD construct comprises amino acids 68−328 (Figure 1). The corresponding cDNA was obtained by PCR and cloned into *Nde*I and *Bam*HI sites of pET-30b plasmid (Novagen). This construct was checked by sequencing and used to transform *E. coli* BL21(DE3) cells. Culture was

initiated from a 5% dilution of an overnight culture into Luria−Bertani medium with 50 mg/L kanamycin. Cells were grown for 3 h at 37 °C, and Lg ECD expression was induced by addition of 100 μM IPTG for an additional 3 h. Cells were harvested by centrifugation at 5000*g* for 20 min. The protein was expressed as inclusion bodies.

Protein Purification. Lg S-CRD and Se-labeled Lg S-CRD were one-step purified with the same protocol, on a streptactin superflow column (IBA GmbH), as previously described (*16*).

Since langerin ECD was expressed as inclusion bodies, a refolding step was required prior to the purification procedures. The pellet obtained from a 3 L culture was resuspended into 50 mL of buffer A (150 mM NaCl, 25 mM Tris, pH 7.8, and 4 mM $CaCl_2$). Cells were lysed by freezing at −20 °C, thawing, and sonication with addition of one complete EDTA-free tablet (Roche Diagnostics). Inclusion bodies were isolated by centrifugation at 10000*g* for 15 min at 4 °C. Refolding was performed by dilution and dialysis as previously described (*9*). Purification of functional Lg ECD proteins was achieved by affinity chromatography on a mannan−agarose column (Sigma) equilibrated in buffer A and eluted in same buffer without $CaCl_2$ but supplemented with 10 mM EDTA (buffer B). This step was followed by a Superose 6 size exclusion chromatography equilibrated in buffer A.

Retardation Assay. The Lg S-CRD functionality was tested by injecting 250 μg of purified protein on a 10 mL mannose−agarose column (Sigma). Equilibration and elution were performed in 150 mM NaCl, 25 mM Tris, pH 8, and 4 mM $CaCl_2$ buffer. As a control experiment 250 μg of bovine serum albumin (Sigma) was injected in the same conditions.

Crystallization, Data Collection, and Processing. Lg S-CRD and Se-labeled Lg S-CRD were crystallized in the same conditions as previously described (*16*). A 0.07 × 0.05 × 0.15 mm crystal of Se-labeled Lg S-CRD was cryoprotected in Paratone-N (Hampton Research) and was flash-frozen in liquid nitrogen. X-ray diffraction data were collected at FIP BM30A beamline at ESRF Grenoble. The peak (λ = 0.98009 Å) and inflection (λ = 0.98025 Å) wavelengths of the Se K adsorption edge were selected based on fluorescence from the crystal. Data sets of 360 images were collected at each wavelength with an oscillation range of 0.5° per image and an exposure time of 40 s. The crystal-to-detector distance was 256.18 mm. Data were processed using the program XDS (*19*). Se-labeled crystals are isomorphous to the native ones (*16*). Diffraction data, including previously collected native data (*16*), were merged using the program CAD from the CCP4 package (*20*).

Phasing, Model Building, and Structure Refinement. First steps of structure determination were performed using the program autoSHARP (*21*). Matthews coefficient determination (*16*) suggests that the asymmetric unit contains either three or four molecules. A MIRAS structure determination was performed using the native data set (*16*) and the two Se derivative data sets (peak and inflection). As there are two diselenium bridges per molecule, each forming one heavy-atom "supersite", and because the asymmetric unit may contain either three or four molecules, six selenium sites were initially searched and eight supersites were finally found. The electron density maps and the initial model resulting from autoSHARP were used as the starting point for model building. The structure refinement was performed on the native data set by cycling between manual building using the program COOT (*22*) and energy minimization with the program REFMAC 5 from the CCP4 package (*20*). Statistics of structure refinement for the native data set are summarized in Table 1.

Table 1: Lg S-CRD Data Collection and Structure Refinement Statistics

Data Collection Statistics for Se-Labeled Crystal		
data set	peak	inflection
wavelength (Å)	0.980089	0.980252
space group	$P4_2$	$P4_2$
unit cell parameters (Å)	a = b = 79.81, c = 90.13	a = b = 79.86, c = 90.15
resolution (Å)	50−2.15 (2.27−2.15)[a]	50−2.15 (2.27−2.15)
measured reflections	229732 (35243)	230246 (35708)
unique reflections	60525 (9451)	60639 (9585)
completeness (%)	99.3 (96.1)	99.5 (97.6)
$I/\sigma(I)$	13.7 (5.1)	14.3 (4.7)
R_{merge}[b] (%)	8.2 (24.8)	8.6 (29.1)
Structure Refinement Statistics for Native Data (*16*)		
resolution (Å)	50−1.5 (1.59−1.5)	
refinement factors		
used reflections/free (%)	84765/5.01	
R_{cryst}[c]	0.189	
R_{free}[c]	0.236	
rmsd from ideality		
bond lengths (Å)	0.014	
bond angles (deg)	1.516	
Ramachandran plot (%)		
most favored regions	86.4	
additional allowed regions	13.6	
generously allowed regions	0.0	
disallowed regions	0.0	
average *B*-factor (Å^2)		
main chains	17.7	
side chains	19.1	
all protein atoms	18.4	
waters	33.4	
all atoms	20.9	
rms B for main chain	0.8	
rms B for side chain	1.6	

[a] Values into parentheses are for the highest resolution shell. [b] $R_{merge} = \sum_h\sum_m|I_m(h) - \langle I(h)\rangle|/\sum_h\sum_m I_m(h)$. [c] $R_{cryst} = \sum||F_o| - |F_c||/\sum|F_o|$, and $R_{free} = R_{cryst}$ calculated with 5% of F_o sequestered before refinement.

Stokes Radius Determination of Langerin Extracellular Domain by Gel Filtration. Superose 12 (Amersham) was calibrated with a mixture of well-characterized proteins with known R_S (gel filtration calibration kits; GE Healthcare). The column was equilibrated in buffer A for 2 column volumes at a 0.8 mL/min flow rate. Dextran blue and FAD were run to determine dead and total volume of the column. Independently, a sample of 0.2 mg of Lg-ECD was also run on the column. All proteins eluted as single peak, and their elution volumes allowed the calculation of the K_{av} by the equation:

$$K_{av} = (V_e - V_0)/(V_t - V_0)$$

V_e being the sample elution volume, V_0 the dead volume, and V_t the total volume. The known Stokes radius of each control proteins allowed to plot a calibration curve, log R_S as a function of K_{av}.

Analytical Ultracentrifugation. Sedimentation velocity experiments were performed at 42000 rpm and 20 °C, using an AN-60 rotor in a Beckman XL-I analytical ultracentrifuge, with two samples of 100 and 400 μL of Lg-ECD at 0.84 mg/mL ($A_{280} \approx 1.6$) and 0.09 mg/mL in 0.3 and 1.2 mm path length cells, equipped with quartz windows, respectively.

Solvent was buffer B. Scans were recorded overnight every 6 min at 280 nm. Data were analyzed using the programs SEDFIT and SEDPHAT (www.analyticalultracentrifugation.com) in terms of a continuous distribution $c(s)$ of sedimentation coefficients, s, and one noninteracting particle (*23*). The solvent density, $\rho = 1.007$ g/mL, viscosity, $\eta = 1.033$ mPa·s, and partial specific volume of langerin, $\bar{v} = 0.734$ mL/g, were estimated from composition with the program SEDNTERP (www.jphilo.mailway.com) and used to derive corrected sedimentation coefficients, $s_{20,w}$. The Svedberg equation relates s to protein molar mass, M, and Stokes radius, R_S: $s = M(1 - \bar{v}\rho)/(N_A 6\pi\eta R_S)$ (with N_A being Avogadro's number). Values for globular compact monomer and dimer were calculated with $R_S = f/f_{min}R_{min}$, R_{min} being the minimum theoretical value for R_S.

Molecular Modeling. The AutoDock 3.0 program (*24*) was used for docking carbohydrate ligands in langerin. Receptor input files were generated using SYBYL 7.3 for the four langerin molecules present in the asymmetric unit. Hydrogen atoms were added and partial charges assigned using AMBER all-atom charges. Hydrogen atom positions were optimized using TRIPOS force field (*25*). Polar hydrogens were differentiated from nonpolar hydrogens using 12-10 and 12-6 hydrogen-bonding Lennard-Jones parameters, respectively. Additional atom type was defined for calcium ion using Åqvist parameters as recently described (*26*). Carbohydrate ligands were built using SYBYL 7.3, and partial charges were taken to PIM parameters for the TRIPOS force field (*27*). All possible torsions in ligand molecules, including hydroxyl groups, were defined as flexible. Grid spacing was set to 0.375 Å. Two different docking tests were assayed: the first one included only the space around the calcium while the second one included the whole monomer. Each single docking experiment consisted in 100 runs employing a Lamarckian genetic algorithm with default parameters except for the number of energy evaluations, set to 1×10^6. The rms deviation tolerance for cluster analysis was set to 1 Å. The molecular model of the trimer was built by homology method, using the COMPOSER program (*28*). The longest identified trimeric coiled-coil, that of influenza virus hemagglutinin (1QU1) (*29*), was used as a template for building the trimeric neck region of langerin. The junction with the CRD domain was obtained by similarity with the MBP-A structure, another trimeric C-type lectin (1RTM) (*30*). Hydrogen atoms were added to the model and final energy minimization included geometry optimization of side chains.

LC Isolation from Human Skin. Human epidermal cell suspensions were obtained from normal skin of patients undergoing abdominal reconstructive plastic surgery after patient-informed consent and according to institutional guidelines. Skin was split-cut with a keratome set and the dermo-epidermal slices were treated for 18 h at 4 °C with 0.05% trypsin in HBSS without Ca^{2+} and Mg^{2+}. The epidermis was detached from the dermis with fine forceps. Epidermal cell suspensions were obtained by subsequent tissue dissociation and filtration through sterile gauze. Basal keratinocytes were removed by adhesion on collagen type I-coated plates (Corning-Iwaki Glass). Partial enrichment was obtained by density gradient centrifugation on Pancoll (Pan Biotech GmbH) which yielded 20−50% $CD1a^+$ LC based on 10 experiments.

Cloning of Langerin Constructs Used in Transfection Studies. Deleted forms were obtained by PCR performed on langerin cDNA (*2*). Primers were designed to amplify fragments incorporating a *Sal*I site followed by the Kozak sequence in the 5′ untranslated region and a stop codon followed by a *Not*I site to the 3′ end. Primers for "Lg ΔCRD" defined a 611 bp fragment comprising residues 1−188 of langerin. Primers for "Lg ΔCyto" defined a 929 bp fragment comprising residues 29−328 of langerin. Mutagenesis was performed using the "gene editor in vitro site-directed mutagenesis" (Promega). A primer containing the P23I mutation was designed to create a silent *Bam*HI restriction site that was subsequently used as a screen to detect mutated clones. All PCR were performed for 35 cycles (1 min denaturation at 94 °C, 1 min annealing at 60 °C, and 2 min elongation at 72 °C) with Taq polymerase. PCR products were then purified using the Wizard prep system (Qiagen), and ligations in pCRII-TOPO vector (Invitrogen) were performed. Putative positive clones were sequence checked. cDNA encoding mutated and deleted langerin forms were then transferred in pMET7 vector using the rapid DNA ligation kit (Boehringer).

Transfection and Expression of Langerin Constructs in COP5 Cells. Murine fibroblastic COP5 cells were cultured in RPMI 1640 supplemented with 10% heat-inactivated fetal bovine serum (FBS), 10 mM HEPES, 2 mM L-glutamine, 50 μM 2-mercaptoethanol, and gentamycin (80 μg/mL). The cells were then electroporated with the langerin expression constructs. Langerin expression was evaluated by FACS analysis.

Cytofluorometry Analysis. COP5 transfected cells were incubated with DCGM4 mAbs (*31*) (10 μg/mL; Beckman Coulter) or with anti-Lag mAbs (*32*) (Becton Dickinson). mAbs were revealed with goat anti-mouse Ig-FITC conjugated (Becton Dickinson). Intracellular staining was performed in the presence of permeabilization medium (0.3% saponin, 2% BSA). Negative controls were performed with an isotype Ig control. Fluorescence was analyzed with a FACScan flow cytometer (Becton Dickinson). Mortality was evaluated using PI incorporation (Sigma).

Transmission Electron Microscopy. After washing, isolated LCs or COP5 fibroblasts transfected with langerin cDNA were fixed with 2% glutaraldehyde in cacodylate buffer for 18 h. After being rinsed in cacodylate buffer with sucrose for 12 h, the cells were processed for transmission electron microscopy. Cells were postfixed with an aqueous solution of 1% osmium tetroxide in cacodylate buffer with sucrose and embedded in epoxy medium after dehydration through a graded series of ethanol. Ultrathin sections were stained with lead citrate and uranyl acetate and examined with a JEOL 1200EX electron microscope with acceleration voltage of 80 kV (Centre des Microstructures, Lyon University, France).

RESULTS

Langerin CRD and ECD Production and Purification. The truncated forms of langerin used in this study are presented in Figure 1a. Lg S-CRD was expressed as a soluble form in the *E. coli* periplasm. The strep-tag II purification tag allowed one-step purification to homogeneity (Figure 1b). The protein functionality was assessed on a mannose−agarose column

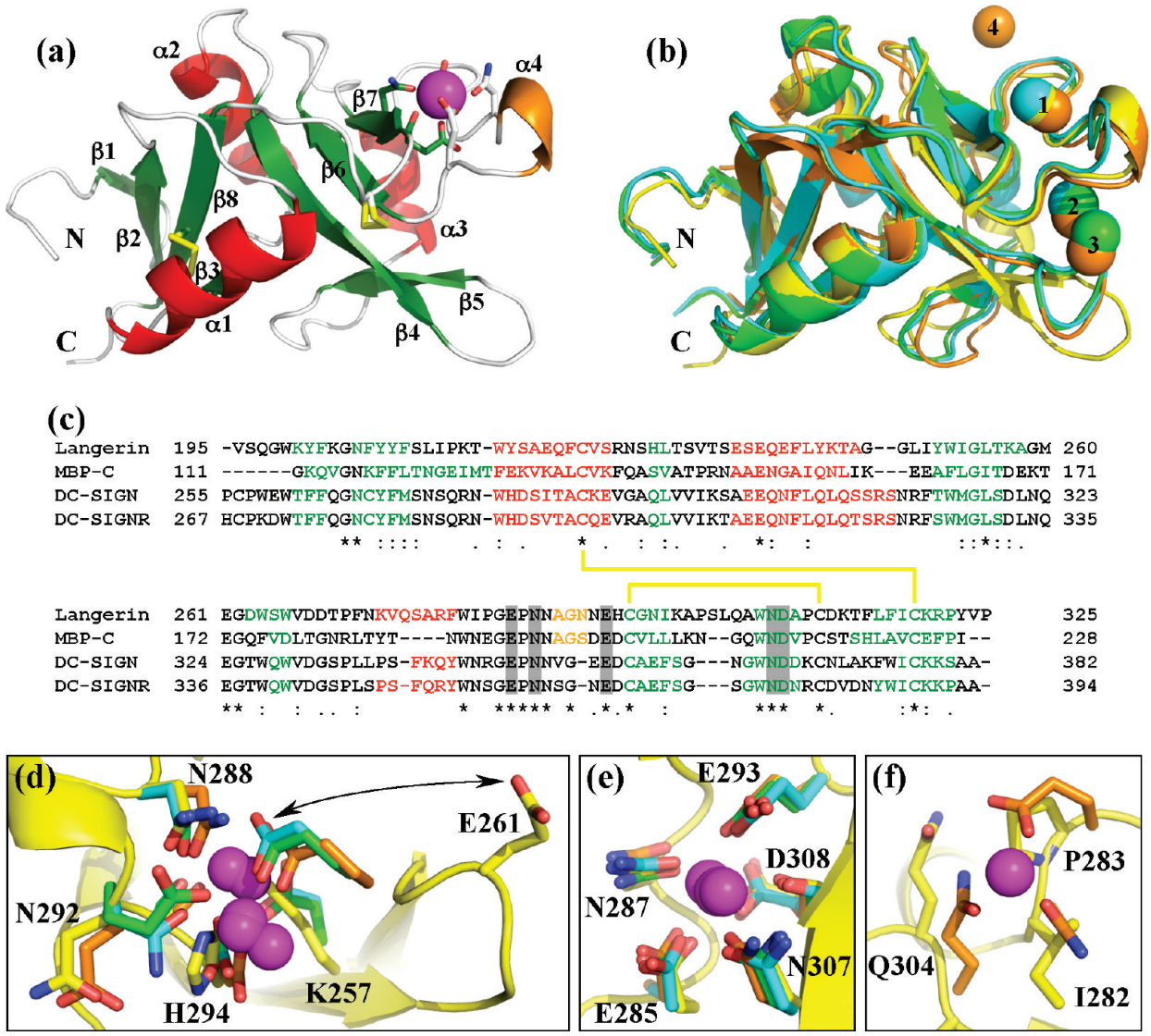

FIGURE 2: Langerin S-CRD structure comparison with other C-type lectin CRDs and structural analysis of langerin calcium-binding site. (a) Structure of Lg S-CRD. α-Helices are shown in red, 3_{10}-helix in orange, *β*-strands in green, loops in white, disulfide bridges in yellow, and Ca^{2+} atom in magenta. Side chains of residues involved in calcium binding are shown as sticks. (b) Superimposition of human langerin (3C22 in yellow), MBP (1HUP in orange), DC-SIGN (1K9I in green), and DC-SIGNR (1K9J in cyan) CRD structures. Numbering indicates calcium-binding sites. (c) Sequence alignment of CRD visible residues in structures of human langerin, MBP, DC-SIGN, and DC-SIGNR obtained from the ClustalW multiple alignment software (www.ebi.ac.uk/Tools/clustalw/index.html). DSSP predicted secondary structures (from DaliLite results) are shown with the same color code as in (a). Conserved disulfide bridges appear in yellow lines. Identical residues are indicated by a "*", conserved substitutions by a ":", and semiconserved substitutions by a ".". Conserved residues binding the carbohydrate interacting Ca^{2+} are highlighted in gray. (d) Region of calcium sites 2 (in back) and 3 (in front). Double arrow indicates Glu261 displacement due to *β*4−*β*5 loop shift. (e) Region of calcium site 1. (f) Region of calcium site 4. The structural representations were drawn with the PyMol program (www.pymol.org).

where langerin CRD elution is delayed whereas the bovine serum albumin, used as a control protein, elutes in the dead volume (Supporting Information Figure 1a).

Langerin extracellular domain (Lg ECD) was produced without an affinity tag. Its oligomeric nature allowed tight binding, through an avidity-based mechanism, on a mannan−agarose column (Supporting Information Figure 1b). Elution required EDTA, demonstrating that binding is calcium dependent and that the Lg ECD has been functionally refolded. Again, this construct was obtained to homogeneity by one-step purification (Figure 1c).

Langerin CRD Structure. The selenium derivative crystal was isomorphous to the native one (*16*). Data processing and refinement statistics are reported in Table 1.

The refined structure constructed from the native data set and the autoSHARP model, obtained from MIRAS phasing, was validated by the program PROCHECK (*33*). The resulting Ramachandran plot showed that 86.4% residues are in the most favored regions, 13.6% residues are in the additional allowed regions, and no residues are in generously allowed regions nor disallowed regions. The asymmetric unit is composed of four monomers related by noncrystallographic 222 point group symmetry. Depending on the monomer, the first 21−24 residues of Lg S-CRD, containing notably the strep-tag II, were absent from the structure. At the C-terminus only three residues are missing except in chain D where the carboxyl terminus was fixed by the two water molecules fulfilling Ca^{2+} coordinations of the chain A carbohydrate-binding site.

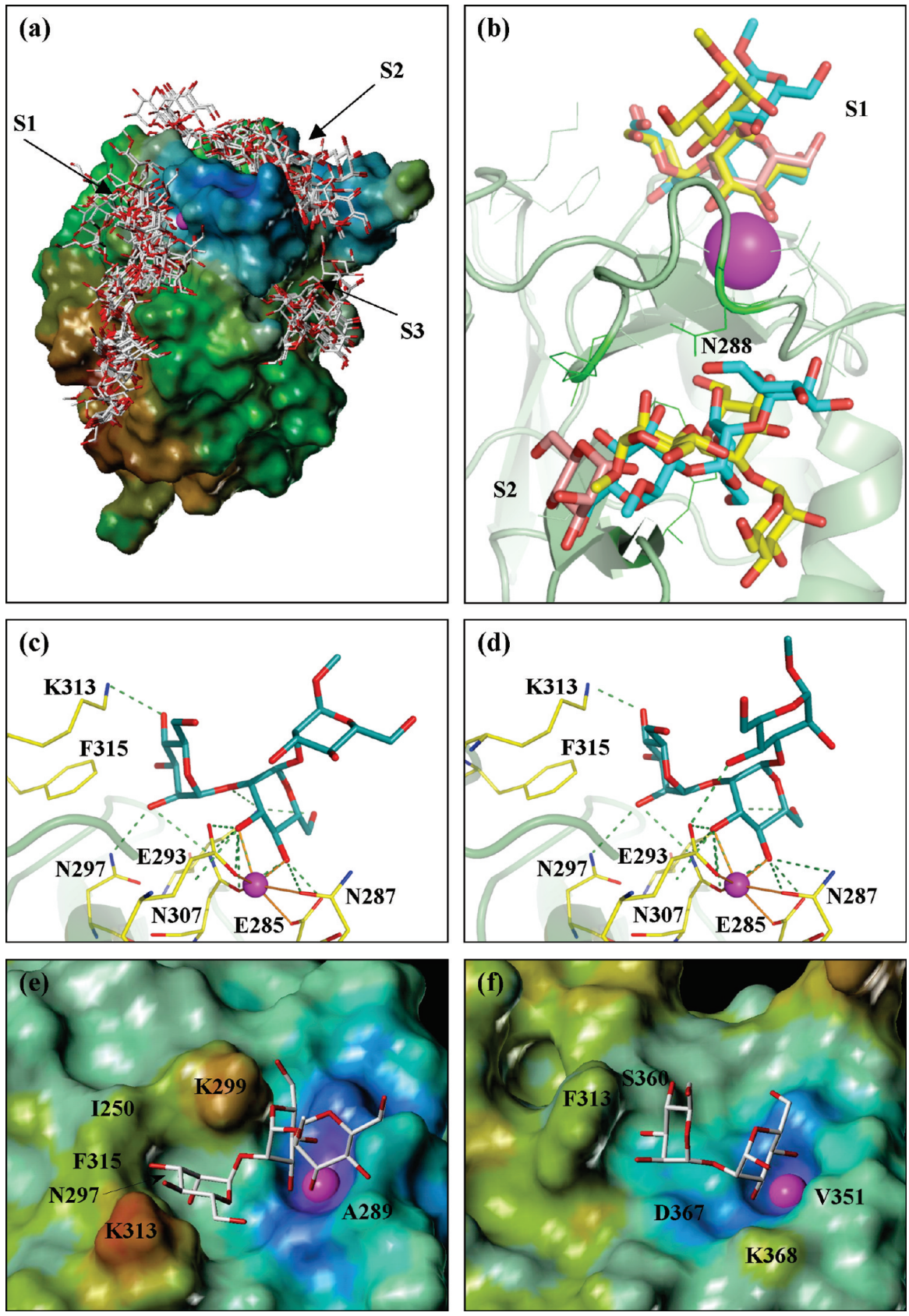

FIGURE 3: Modeling of oligosaccharide interaction with langerin CRD. (a) All predicted orientations for M12M12M represented on the accessible surface of langerin CRD color-coded according to lipophilic potential, polar (blue) to hydrophobic (brown). S1 and S2 are high probability sites; S3 is a low probability site. (b) Lower energy docking modes for M12M12M (cyan) and M12M13M (yellow) in sites S1 and S2. The mannose residue reported in the crystal structure of langerin CRD (*15*) is also represented (salmon). In the S2 site, side chains in green represent amino acids involved in oligosaccharide binding. (c, d) Lower energy docking modes in the calcium-binding site for M12M12M and M12M13M, respectively. (e) Lower energy docking modes for M12M12M together with accessible surface of langerin CRD color-coded according to electrostatic potential, acidic (blue) to basic (red). (f) Same representation for the structure of α-D-mannose-(1−2)-α-D-mannose in DC-SIGN site (2IT6).

Table 2: Hydrodynamic Properties of Lg ECD and Trimeric Model[a]

	Lg ECD		trimeric model
	analytical ultracentrifugation	gel filtration	HYDROPRO calculation
$s_{20,w}$ (S)	4.05 ± 0.1	na	3.9
R_S (nm)	5.1 ± 0.06	5.13 ± 0.3	5.4
ff_{min}	1.73 ± 0.02	na	1.8

[a] $s_{20,w}$, sedimentation coefficient; R_S, Stokes radius; ff_{min}, frictional ratio; na, not applicable.

Langerin CRD structure was compared with the structures of human mannose-binding protein (MBP) CRD (1HUP), DC-SIGN CRD (1K9I), and DC-SIGNR CRD (1K9J). At first sight, the overall structure of langerin CRD (Figure 2a) roughly observes the classical conserved fold and features of C-type lectins as illustrated by the aligned structures and sequences (Figure 2b,c). A more precise view pinpoints some specific features. Like MBP, langerin has a 3_{10}-helix near the carbohydrate-binding calcium site that is not conserved in DC-SIGN nor in DC-SIGNR structures. Additional differences concern calcium-binding sites. Only the carbohydrate-binding calcium site was conserved in langerin CRD (site 1 in Figure 2b,e) whereas site 4 was lost due to amino acid variations (Figure 2f). For sites 2 and 3 the changes are larger, implicating β4 and β5 strands, β4−β5 loop, and some residue modifications (Figure 2d). Only Asn288 was conserved, Asn292 was shifted out of the site, and at positions 294 and 257 aspartates are replaced by a histidine and a lysine, respectively. Lys257 side chain occupies the classical calcium site 2. As a consequence the β4−β5 loop, containing Glu261, is shifted far from its canonical position leading to a large groove specific to the langerin structure.

Molecular Modeling of Langerin/Oligosaccharide Complexes. A docking approach recently developed for calcium-mediated protein−carbohydrate interactions (*26*) has been used for predicting the binding mode of oligosaccharides on langerin. It has been shown that langerin can bind HIV-1 and HIV-2 gp120 proteins in a mannan-inhibitable manner (*12*), supporting gp120 glycan recognition. Moreover, data publicly available from the Consortium for Functional Glycomics [www.functionalglycomics.org/glycomics/publicdata/selectedScreens.jsp] confirm the affinity for oligomannosides. Indeed, glycan array data using the Lg-ECD or the Lg-CRD (report to data, on the consortium Web site, from G. Zurawski group and A. Skerra group, respectively) indicate that the high-mannose type N glycan, abundantly expressed on gp120 (*34*), and its derivative oligosaccharide, αMan12αMan12αMan13Man, are among the best ligands for langerin. Consequently, two linear mannosidic fragments were considered, i.e., αMan12αMan12αManOMe (M12M12M) and αMan12αMan13αManOMe (M12M13M). The docking calculation was not limited to the calcium-binding site but included the whole CRD. When looking at the complete docking results, i.e., 100 solutions, three preferred binding regions are identified at the protein surface, for both trisaccharides, as displayed in Figure 3a for M12M12M. The S1 site corresponds to the calcium-binding site but also extends for a few nanometers, indicating that longer oligosaccharides could interact. The S2 binding site corresponds to the groove created by the unusually opened β4−β5 loop (Figure 3b). This very hydrophilic region, corresponding to calcium sites in most C-type lectins, contains many residues

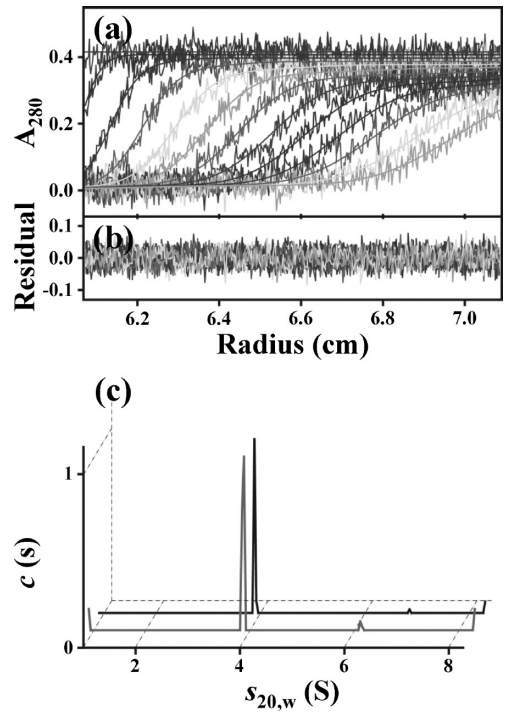

FIGURE 4: Langerin ECD sedimentation velocity analysis. (a) Superimposition of selected experimental and modeled profiles obtained at 20 °C, in 3 mm path-length cell, for up to 6 h at 42000 rpm for langerin at 0.84 mg/mL; the analysis was done without regularization and using systematic noise subtraction, considering 200 particles between 1 and 8 S with a fitted frictional ratio of 1.6. (b) Related residuals. (c) $c(s)$ for langerin at 0.84 (gray curve) and 0.09 mg/mL (black curve); $c(s)$ scale is normalized to a maximum value of 1 and shifted for the latter.

favorable to carbohydrate binding (asparagine, histidine, tryptophan) and has indeed been reported as a secondary mannose-binding site in the recent structure of langerin CRD (*15*). A third binding region, labeled S3, is close to S2, albeit with less favorable binding energies for oligosaccharides.

The most populated clusters (23% for M12M12M and 67% for M12M13M) correspond to the classical conformation with the central mannose residue coordinated to the calcium through its O3 and O4 hydroxyls (Figure 3c,d; see also Supporting Information Tables 1−3). The orientation of this residue is similar to the one observed for mannose alone in langerin (*15*) and mannose-binding proteins (*35, 36*). The nonreducing α1−2-linked mannose fits in a pocket adjacent to the main binding site and establishes hydrogen bonds with Asn297 and Lys313 (Figure 3c−e). Additional stabilization is provided by van der Waals contact between H−C4 and the Phe315 aromatic ring. On the contrary, the mannose on the reducing end does not make significant contribution to the binding, independently to its linkage with the calcium-bridged one (1−2 or 1−3 linkage).

Langerin ECD Hydrodynamic Studies. Stokes radius of langerin extracellular domain was estimated by migration over a Superose 12 size exclusion column, and an experimental Stokes radius of 5.13 nm was obtained (Table 2). This R_S value would correspond to a molecular mass of 243 kDa for a globular hydrated protein. The discrepancy with the theoretical mass of 88.2 kDa for the langerin ECD organized as a trimer, as previously described (*9*), strongly suggests a very elongated structure for langerin ECD.

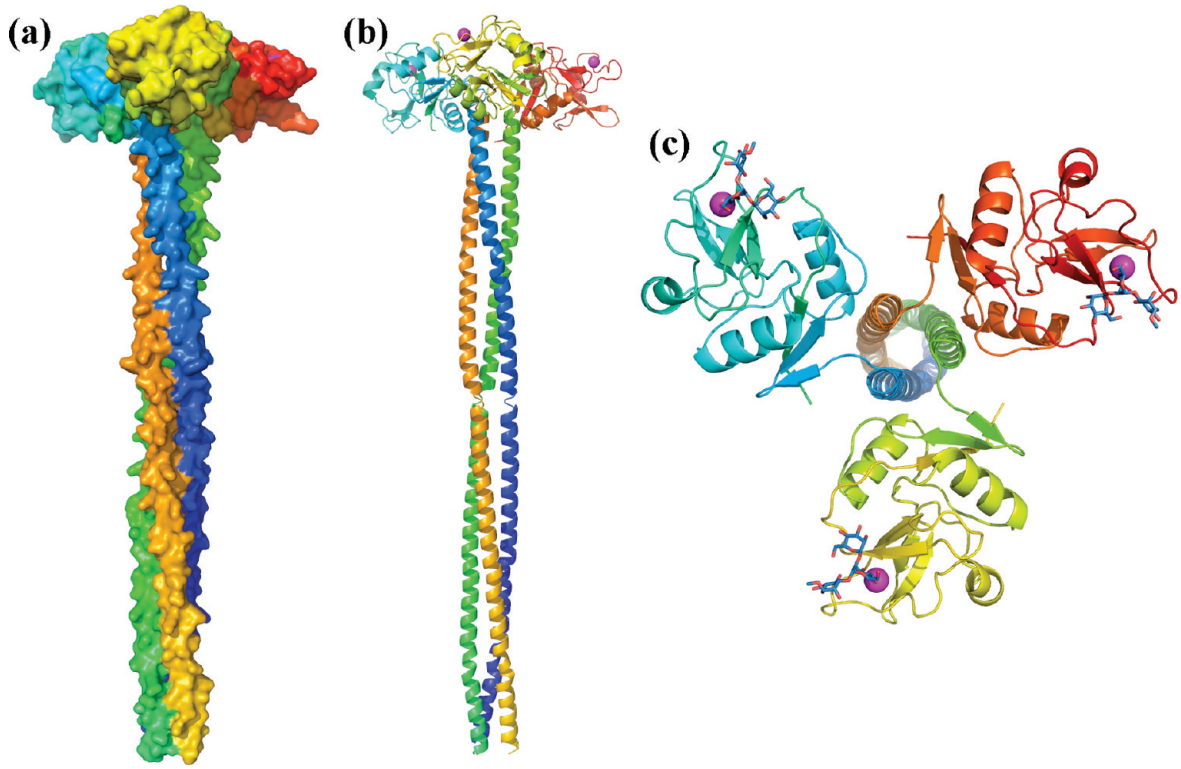

FIGURE 5: Langerin ECD trimer model. (a) Surface side view. (b) Cartoon side view. (c) Cartoon top view. Color code: rainbow colored langerin, magenta colored Ca^{2+} atom. The trimannoside M12M12M, sky blue colored, was not included in the modeling of the Lg-ECD but has been added in the figure to help visualize the interaction site of the protein.

Analytical ultracentrifugation sedimentation velocity experiments (Figure 4) were performed to confirm the association state and the Stokes radius of langerin. For samples at 0.84 and 0.09 mg/mL, the $c(s)$ analysis showed an essentially homogeneous sample with a species at $s_{20,w}$ = 4.03 S. The two data sets were thus globally analyzed with the program SEDPHAT, which provided an estimation of $s_{20,w}$ = 4.07 S and of the molecular mass = 83 kDa (the same value was obtained starting the fit with the hypothesis of a dimer of 58 kDa or a trimer of 88 kDa) in agreement with a trimer in solution. Combining the value of $s_{20,w}$ = 4.05 S with the mass of the trimer provided a Stokes radius value, R_S, of 5.1 nm as obtained with size exclusion chromatography (Table 2). The related frictional ratio of 1.7 corresponds to a very anisotropic shape, values for globular compact proteins being typically 1.25 ± 0.05. A strong correlation is thus observed between both size exclusion chromatography and velocity experiment analysis and suggests a very elongated shape for the langerin ECD.

Langerin ECD Structure Modeling. The neck region, involved in the trimerization, is a classical α-helix coiled-coil region as confirmed by sequence analysis using the COILS program (www.ch.embnet.org/software/COILS_form.html (*37*), data not shown) and by previously reported circular dichroïsm spectroscopy studies on langerin (*9*). Parts of influenza virus hemagglutinin (1QU1) and MBP-A trimeric structure (1RTM) have been used as templates for molecular modeling of trimeric ectodomain of langerin as described in Experimental Procedures. The resulting model is presented in Figure 5. The molecule is fairly elongated with the long axis extending over 20 nm. The coordinates were used as an input file in the HYDROPRO program (*38*) to calculate a theoretical Stokes radius. A value of R_S = 5.3 nm was obtained. This is in good agreement with the experimental values determined by size exclusion chromatography and sedimentation velocity (Table 2). It is also remarkable that the calculated frictional ratio is in good agreement with experiment. These strong correlations strengthen confidence in the very elongated langerin ECD structural model. The fact that the calculated frictional ratio is slightly larger than the experimental one (1.8 instead of 1.73) can be easily rationalized by the existence of flexibility of the elongated molecule, which is not taken into account in the rigid model.

Birbeck Granule Formation and Membrane Remodeling: Model of Langerin Extracellular Domain Organization. In order to propose a working model for langerin ECD contribution to BG organization, we observed numerous sections of freshly isolated Langerhans cells. As previously described, all BGs exhibit electron-dense paracrystalline structures in the center of a membrane sandwich (*39*), hereafter termed CMS for "cytomembrane sandwiching" structures. From Figure 6a, no electron-dense paracrystalline or even individual structure is visible on membranes adjacent to the BG formation site. This suggests that appearance of such structures is dependent on symmetrical elements, emerging from facing membranes. The association of these elements (involving an external ligand or not) could result in a bigger central object. Such higher order structure would then be visible, in this negative staining mode, in the center of the sandwiched membrane. Depending on the BG sections and on the membrane limits used for the estimation, the width of the BG zippered membranes can be evaluated in a range of 25−40 nm (Figure 6b).

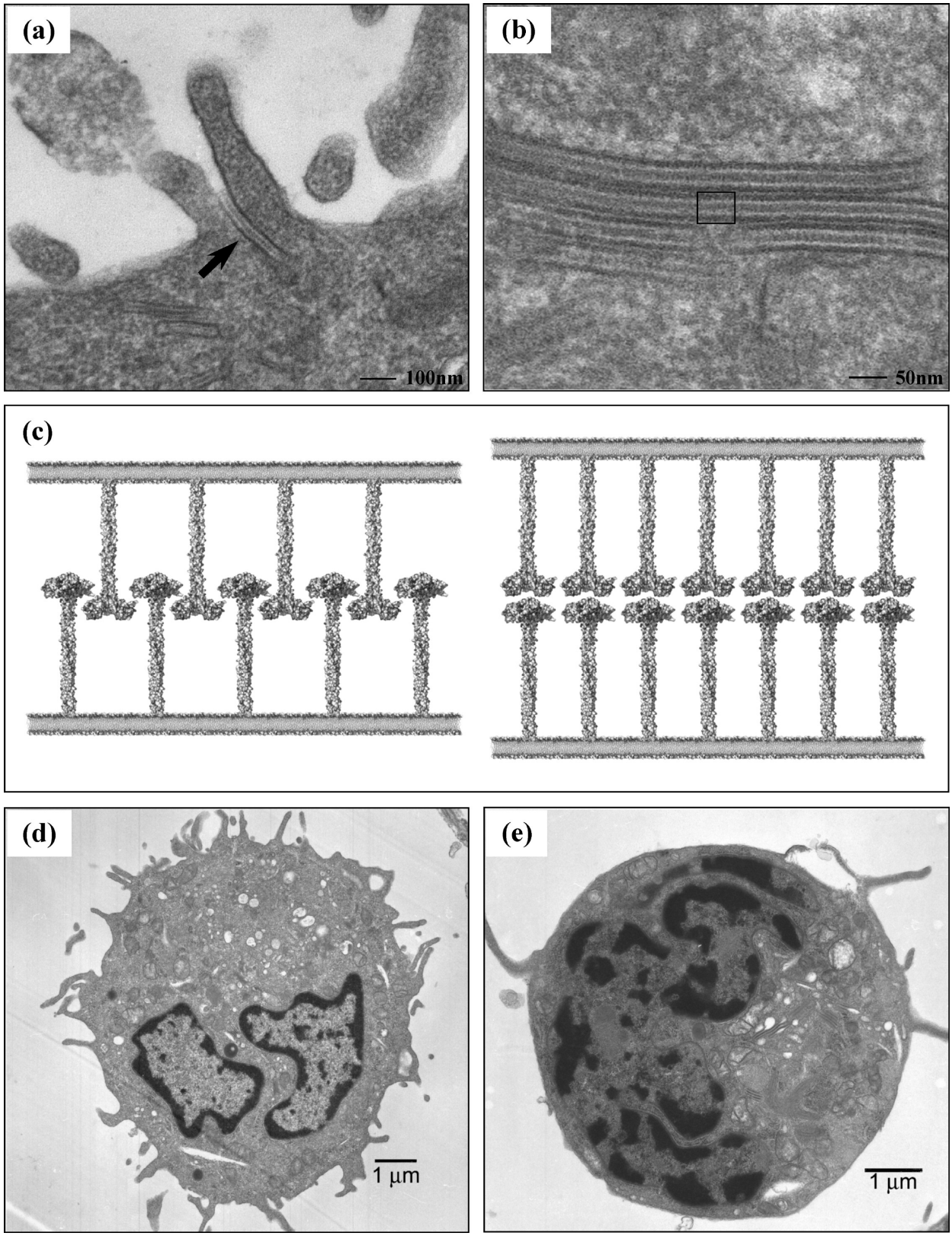

FIGURE 6: Birbeck granules in Langerhans cells and proposed macromolecular organization models. (a) Plasmic membrane invagination forming a cytomembrane sandwiching structure (CMS) (arrow) in a fresh isolated LC. (b) Stacked Birbeck granules of LC. (c) Two proposed Birbeck granule macromolecular organization models. (d, e) Langerin triggering inducing LC remodeling and Birbeck granule formation. LCs were incubated with mAb DCGM4 (e) or with anti-CD1a as control (d). A clear induction of intracellular BGs is observed in the pericentriolar region of DCGM4 treated cells, the dendritic cell shape is lost, and no dendrites can be observed.

From these various observations and from the langerin architecture deduced from sequence analysis, modeling, and hydrodynamic studies, we propose putative working models for the contribution of the langerin C-type lectin to the ultrastructural organization of the BG (Figure 6c). In such models, the CRDs displayed by facing membranes could

correspond to the central electron-dense structure. The dimensions of this model are compatible with the distances estimated from electron microscopy images.

More strikingly, we observed on fresh isolated LC that CRD engagement by DCGM4 mAb induces accumulation of BGs in the pericentriolar region (Figure 6e and Supporting Information Figure 2b). No such effect was observed with an isotype control (data not shown) or anti-CD1a mAb (Figure 6d and Supporting Information Figure 2a). Moreover, this triggering of langerin CRD also induces morphological changes: LCs become rounded and lose their dendrites (Figure 6e) compared to anti-CD1a-treated LC (Figure 6d). Besides, mannan triggers the same effect as DCGM4 mAb (data not shown). Taken together, our results demonstrate also the crucial role of the langerin ECD in the vesicle machinery for BG formation and rearrangements of LC morphology.

Langerin Carbohydrate Recognition Domain Is Required for Birbeck Granule Formation. To further explore the role of different domains of langerin in LC membrane rearrangement and BG formation, we generated mutated and deleted forms of human langerin. One form, termed Lg ΔCRD, is devoid of the CRD but retains the neck domain, whereas the second one, termed Lg ΔCyto, was deleted in the intracytoplasmic domain. Finally, langerin contains an intracellular PXXP sequence potentially recruiting SH3 domain containing proteins; therefore, a mutated form was generated with a P23I mutation in this motif (Figure 7a). After transfection in COP5 cells, we analyzed the expression of the different langerin constructs using either mAb DCGM4 for the CRD of langerin or mAb Lag recognizing the intracellular domain (*32*). As shown in Figure 7a, flow cytometry analysis showed that similar transfection efficiency and expression were observed for all constructs. As expected, mAb DCGM4 and mAb Lag reactivity was observed only when the CRD domain or the cytosolic domains are present, respectively.

After transfection in COP5 cells, we also performed electron microscopy and observed that the CRD of langerin is strictly necessary for the formation of BG structure. Indeed, no BG was observed in Lg ΔCRD transfected cells (Figure 7b,c) while BG and BG-related structures (CMS) were obtain with Lg WT as already described (data not shown) (*2*). More strikingly, we observed CMS in Lg ΔCyto transfected cells (Figure 7d). In contrast to Lg WT transfected cells (*2*), these CMS were never connected to vesicles but associated with ribosome-like condensation evoking rough endoplasmic reticulum (Figure 7e). This suggests that the cytoplasmic domain is essential to allow langerin targeting to other compartments. Interestingly, transfection of langerin mutated in the proline-rich motif (WPREPPP) of the cytosolic domain did not impair formation of superimposed membrane structures, but the latter were frequently connected to multivesicular bodies (Figure 7f,g).

Taken together, those mutants further emphasize the role of langerin CRD in the establishment of the definitive paracrystalline ultrastructure of BG.

DISCUSSION

Langerin Structure in the C-Type Lectin Family and Carbohydrate-Binding Mode. The langerin CRD presents some differences with other known C-type lectin structures for calcium binding. Langerin has only one calcium-binding site, corresponding to the canonical carbohydrate-binding site, whereas DC-SIGN/DC-SIGNR and MBP bind three to four calcium ions, respectively. As illustrated in Figure 2c, site 1 ligands (residues highlighted in gray) and the positions of their lateral chain are strictly conserved (Figure 2e), maintaining calcium site 1 integrity. For site 4, only Gln304 is conserved (Figure 2f) whereas for sites 2 and 3 many environmental changes have an obvious impact on the calcium ion loss and allow the large movement of the $\beta4-\beta5$ loop (Figure 2d). Thus a large groove is formed which is specific to langerin and not observed in DC-SIGN/DC-SIGNR or MBP.

Differences are also observed in the calcium-dependent carbohydrate-binding sites (Figure 3e,f). The DC-SIGN-binding site is characterized by the presence of Phe313 that establishes stacking with sugar B face (*40, 41*). In langerin, Phe315 is not in an appropriate position to play the same role. The presence of two lysine residues in langerin site environment, Lys299 and Lys313, is also unique to this CRD. This basic character of the binding site could be correlated with the reported affinity of langerin toward sulfated oligosaccharides (*8*). Our structure is in good agreement with the structure previously reported this year (*15*).

Oligomerization state also influences carbohydrate binding through an avidity-based mechanism. Langerin coiled-coil trimeric association compensates the CRD low affinity by the presentation of three identical carbohydrate recognition domains. Hydrodynamics studies performed on recombinant langerin ECD illustrate the very anisotropic shape of the trimer. The ECD model generated in this work is in agreement with results of the hydrodynamic studies (Table 2) but also with the known characteristics of other lectins with coiled-coil-based multimerization. Indeed, it is very similar to the well-characterized MBP trimeric structure (*30*). Uncertainties mainly reside in the relative flexibility of the different CRD domains with respect to each other.

Our modeling approach predicts that langerin binds to terminal αMan12Man moiety of gp120 in a well-defined extended pocket close to the calcium-binding site (Figure 3e). Search for possible secondary sites results in the identification of an additional region that would be favorable for mannose/oligomannose binding. The S2 binding site, which only occurs in langerin, is of high interest and closely corresponds to the secondary carbohydrate-binding site observed in recently published langerin CRD structures (*15*) (Figure 3b). Furthermore, the Asp288 variant, a result of human langerin polymorphism, has been demonstrated to bind to the mannose column with lower affinity than the major Asn288 form (*42*) (see Figure 3b for Asn288 location in S2 site). In the structure with maltose (*15*) as well as in our oligomannose binding modeling in the S2 site, this Asn288 is potentially involved in carbohydrate interaction. This strengthens the role of this langerin-specific groove in the interaction with carbohydrate and the need for future characterization of this unusual carbohydrate-binding site.

Langerin, DC-SIGN, and HIV. From the initial report on the use of DC-SIGN by HIV as a Trojan horse to invade the host organism, several groups have also shown that DC-SIGN is used by many other pathogens during their corresponding infection process (*43−47*). Hence, generation of DC-SIGN ligands, that can be used to inhibit or explore the

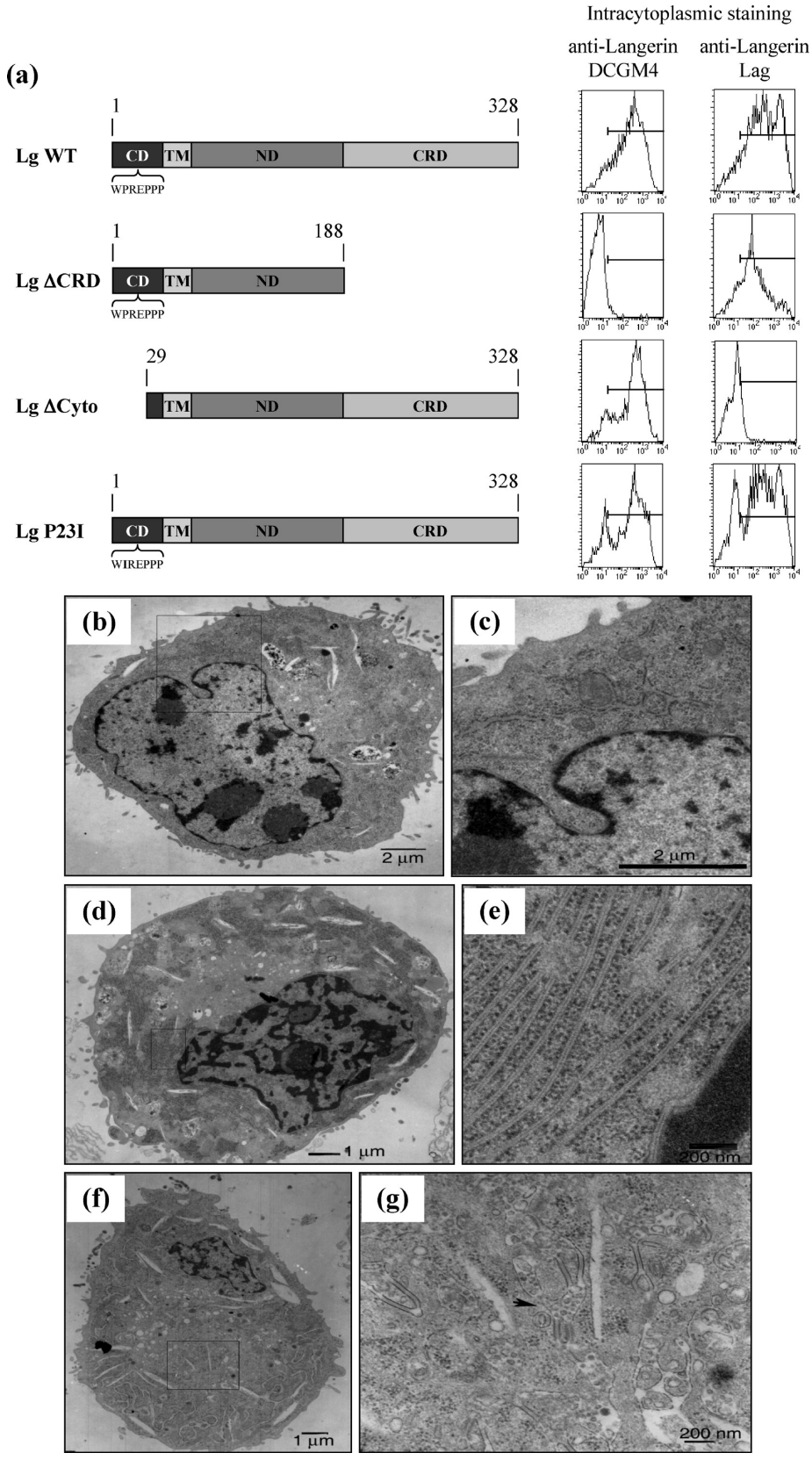

FIGURE 7: Electron microscopy (EM) of BG-related structures after transfection with different forms of human langerin. (a) Schematic representation of human langerin constructs and corresponding FACS staining on transfected COP5 cells using the anti-langerin mAbs DCGM4 and Lag following permeabilization. The Lg ΔCRD form lacks the entire carbohydrate recognition domain. The Lg ΔCyto form is deleted in the intracytoplasmic domain. The Lg P23I form contains a mutation of Pro23 into Ile in the proline-rich motif. (b−g) Electron microscopy performed on langerin COP5 transfected cells. Lg ΔCRD COP5 transfected cells shows no BG formation (b, c), whereas deletion of the intracytoplasmic domain (Lg ΔCyto) results in BG-related structures known as "cytomembrane sandwiching structures" (CMS) (d). These CMS are connected to abundant ribosomes evoking the rough endoplasmic reticulum (e). Mutation in the proline-rich motif (Lg P23I) does not allow induction of genuine BGs but rather multivesicular bodies (MVB, arrowhead) in continuity to CMS (f, g). Zoomed regions in (c), (e), and (g) correspond to squares in (b), (d), and (f), respectively.

role of DC-SIGN in pathogenesis and immunological process, is an important issue (*48*−*53*). The recent highlight on a divergent function between DC-SIGN and langerin with respect to HIV (*54*) might orient future efforts toward the design of molecules able to distinguish these two C-type lectin receptors. Thus, detailed characterization of the two binding sites is of central importance for such strategies. Panels e and f of Figure 3 present a comparison of langerin- and DC-SIGN-binding sites, respectively. In langerin, a well-defined pocket close to the calcium-binding site allows the accommodation of the terminal αMan12Man, found in high-mannose glycans (Figure 3e). DC-SIGN also binds αMan12Man with a similar orientation of the reducing mannose (*55*). However, the extended binding site is very different in the two lectins, and the bound disaccharides adopt different conformations. In DC-SIGN, the second mannose establishes a hydrogen bond with Ser360 and is partially stacked with Phe313. In langerin, Lys299 and Lys313 are directly involved in the interaction and add strong positive charges in this binding site. These two main differences, in topology and charge of the calcium-binding sites, constitute the first elements to envisage future drug design of selective compounds.

In addition to the differences in the two active sites, divergence in the oligomerization and in the binding site presentation may play a crucial role in the recognition. The occurrence of two sugar-binding sites on langerin CRD could participate in high avidity for glycosylated proteins. In both S1 and S2 sites, the oligosaccharide reducing ends are correctly oriented for binding terminal oligosaccharides from glycoconjugates. The distance between the two sites is over 20 Å, which is rather large for binding the two arms of the same biantennary high-mannose. Moreover, when considering the langerin trimeric model (Figure 5c), the estimated distance between two adjacent calcium-binding sites suggests that binding of adjacent CRDs necessarily occurs on different biantennary high-mannose. Nevertheless, gp120, which is the target of langerin on HIV (*12*), presents a shield of glycan on its exposed face (*56*) with many αMan12Man epitopes (*57*). Further characterization of DC-SIGN and langerin, in their oligomeric form, will be required to evaluate the contribution of this state with respect to their behavior toward HIV.

Langerin and Birbeck Granule Biogenesis. Although BGs have been first observed in 1961 (*4*), there is still a large part of mystery around their organization and function in the Langerhans cells. Nevertheless, BGs were described as organelles allowing a nonclassical routing for an antigen-processing pathway in the Langerhans cells (*11, 58*).

More than a simple association, a direct role of langerin in BG formation was demonstrated from observation of BG induction in murine fibroblasts (*2*) as well as in human melanoma cell line (*5*) upon langerin gene transfection. Langerin extracellular region, and more precisely its CRD, was suggested to be a key element in the BG architecture. Using Lg ΔCRD langerin, we observed that the lectin domain is strictly necessary for BG formation. This is consistent with the observation that Ca^{2+} removal can cause unzipping to various extents with inner periodical pattern disintegration (*59, 60*). Furthermore, langerin CRD point mutation W264R induces tubular-like structures different from characteristic structural features of BGs (*61, 62*). This residue is located in the middle of a large hydrophobic cluster in the CRD close to the calcium-binding site. The paracrystalline structure observed in the linear inner lamella of BG could be CRDs, possibly with associated ligands, engaged in a supramolecular organization. The observation of an induction of BG formation, upon triggering of langerin CRD with a specific mAb (DCGM4), is an additional strong argument to this scheme.

The coiled-coil neck regions allow terminal CRD presentation at rather long distances from the membrane surface. In BGs, the central electron-dense lamellar structures present spatial dimensions that are in good correlation with the size of our langerin ECD model (Figure 6b,c). Of course, these latter models are at this stage solely a "working hypothesis". Future experiments will be necessary to affine the dimension of this architecture and to investigate langerin ECD organization in such structures. The requirement of a ligand binding to initiate these high molecular weight assemblies will also need to be demonstrated.

Finally, we observed that transfection of Lg ΔCyto triggers the folding of membranes associated with ribosome-like condensation and evoking rough endoplasmic reticulum. We hypothesize that this deleted langerin mRNA is highly translated, due to the SV40 promoter, resulting in high langerin protein levels but without the correct addressing signal. Indeed, less drastic modification, the P23I mutation in the polyproline motif of the cytoplasmic domain, allows formation of CMS structures that are connected to a multivesicular body instead of genuine BG.

These latter observations demonstrate that the extracellular domain, and more particularly the CRD, is the key player in the membrane zippering as CMS structure. However, emphasis is also brought to the cytosolic domain playing a central role in membrane targeting and BG formation. The intracytoplasmic PXXP sequence is a putative SH3 binding motif, which is found in a number of molecules involved in a wide variety of biological processes (kinases regulation, subcellular localization, signaling pathways, etc.). Indeed, the altered distribution of the CMS structures, resulting from the P23I mutation, suggests the involvement of adaptor proteins. The association of Lg P23I construct with multivesicular bodies, which are protein-sorting stations of the endocytic pathway (*63*), is in accordance with previous studies. Indeed, Mc Dermott et al. have shown that BG can be formed from recycling endosomes (*64*). Both Lg ΔCyto and Lg P23I allow the formation of CMS structure but alter, to different extents, the global localization or organization of these CMS structures as genuine BG further emphasizing a role of the cytoplasmic region in the final organization of BG.

Membrane Deformation Mechanisms. Membrane deformations, for internalization as well as for budding, are crucial for many cell functions. Mechanisms leading to HIV internalization in Langerhans cell involve BG formation, simultaneously to HIV binding, through membrane deformation, invagination, and zipping. We show here that such membrane remodeling, BG formation, and even a global change of LC morphology can be induced (Figure 6) by triggering langerin with mAb DCGM4 which is specific for a CRD epitope overlapping with the calcium-dependent carbohydrate-binding site (*2*). This suggests that glycoconjugate ligands specific for the langerin CRD could be at the onset of the BG formation. Dynamic membrane remodeling

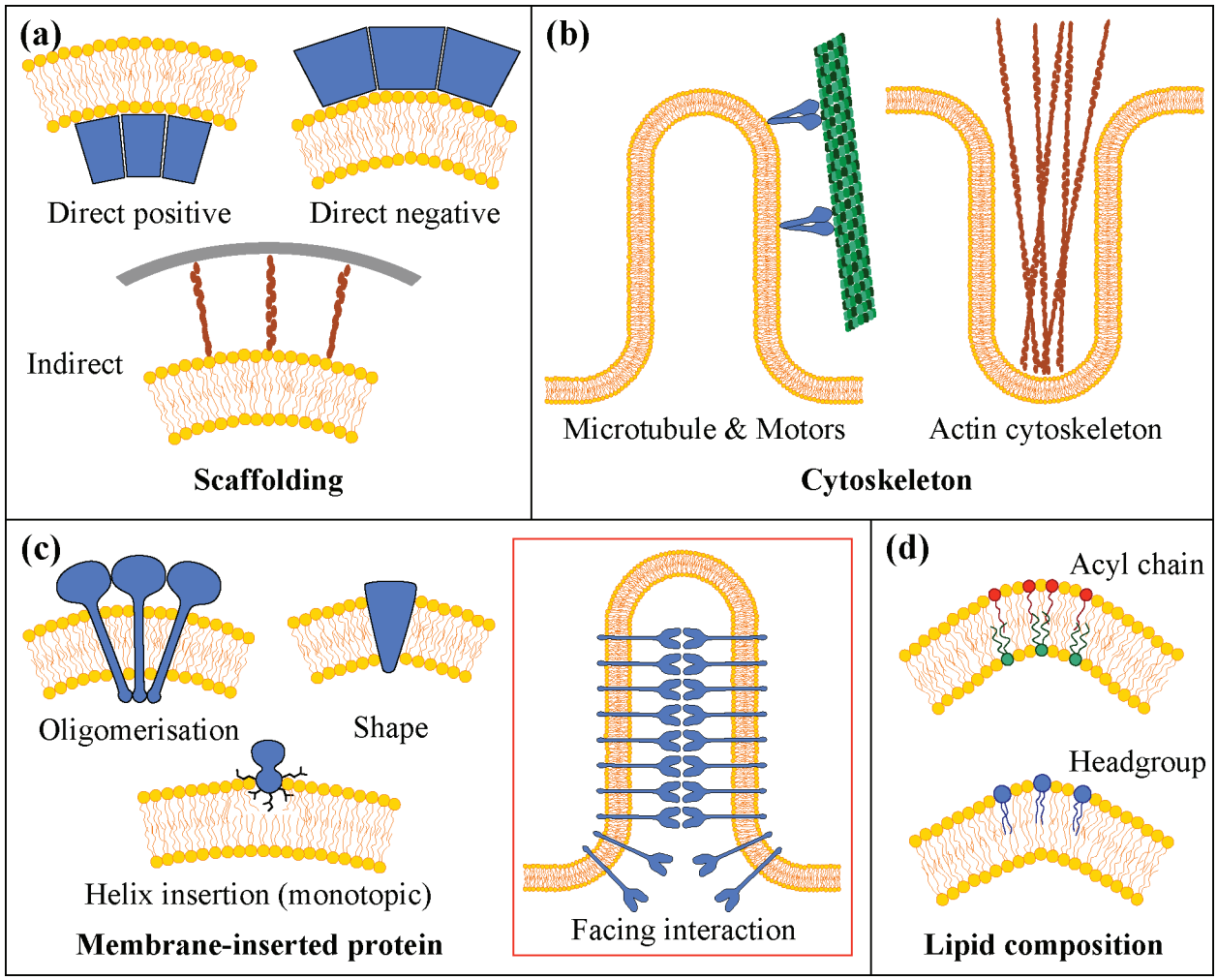

FIGURE 8: Reported membrane deformation mechanisms. (a) Scaffolding caused deformations. (b) Cytoskeleton caused deformations. (c) Membrane protein caused deformations. Red square: model of membrane zipping proposed for Birbeck granule formation. (d) Lipid composition caused deformations.

is classically performed by the interplay between lipids and protein. McMahon and Gallop have reported five general modes of membrane bending: lipid composition, cytoskeletal dependent membrane modeling, scaffolding by peripheral membrane proteins, amphipathic α-helix insertion, and finally bending resulting from the insertion of proteins in the membrane bilayer (see Figure 8, adapted from their review) (*65*). The membrane zipping arising from molecular interactions involving facing langerin receptors induces the deformation by a novel mechanism (Figure 8c, red square).

The requirement of the lectin properties of the langerin, the involvement of specific oligosaccharides and/or glycoconjugates in this membrane zipping, is still to be confirmed. However, the relative importance of the CRD, the coiled-coil region, and the cytosolic domain of langerin in membrane targeting, assembly, and stabilization of such structures has been underlined in this work for the first time.

ACKNOWLEDGMENT

We thank Dr. K. Yoneda for kindly providing anti-Lag antibody. We also thank M. P. Strub for support with selenocysteine/selenomethionine double labeling.

SUPPORTING INFORMATION AVAILABLE

Elution profiles of Langerin CRD and ECD from a mannan agarose column, zoomed sections of Figure 6d,e, and molecular modeling data. This material is available free of charge via the Internet at http://pubs.acs.org.

REFERENCES

1. Bell, D., Young, J. W., and Banchereau, J. (1999) Dendritic cells. *Adv. Immunol. 72*, 255–324.
2. Valladeau, J., Ravel, O., Dezutter-Dambuyant, C., Moore, K., Kleijmeer, M., Liu, Y., Duvert-Frances, V., Vincent, C., Schmitt, D., Davoust, J., Caux, C., Lebecque, S., and Saeland, S. (2000) Langerin, a novel C-type lectin specific to Langerhans cells, is an endocytic receptor that induces the formation of Birbeck granules. *Immunity 12*, 71–81.
3. Geijtenbeek, T. B., Kwon, D. S., Torensma, R., van Vliet, S. J., van Duijnhoven, G. C., Middel, J., Cornelissen, I. L., Nottet, H. S., KewalRamani, V. N., Littman, D. R., Figdor, C. G., and van Kooyk, Y. (2000) DC-SIGN, a dendritic cell-specific HIV-1-binding protein that enhances trans-infection of T cells. *Cell 100*, 587–597.
4. Birbeck, M. S., Breathnach, A. S., and Everall, J. D. (1961) An electron microscope study of basal melanocytes and high-level clear cells (Langerhans cells) in vitiligo. *J. Invest. Dermatol. 37*, 51–63.
5. McDermott, R., Bausinger, H., Fricker, D., Spehner, D., Proamer, F., Lipsker, D., Cazenave, J. P., Goud, B., De La Salle, H.,

Salamero, J., and Hanau, D. (2004) Reproduction of Langerin/CD207 traffic and Birbeck granule formation in a human cell line model. *J. Invest. Dermatol. 123*, 72–77.
6. Valladeau, J., Clair-Moninot, V., Dezutter-Dambuyant, C., Pin, J. J., Kissenpfennig, A., Mattei, M. G., Ait-Yahia, S., Bates, E. E., Malissen, B., Koch, F., Fossiez, F., Romani, N., Lebecque, S., and Saeland, S. (2002) Identification of mouse langerin/CD207 in Langerhans cells and some dendritic cells of lymphoid tissues. *J. Immunol. 168*, 782–792.
7. Takahara, K., Omatsu, Y., Yashima, Y., Maeda, Y., Tanaka, S., Iyoda, T., Clausen, B. E., Matsubara, K., Letterio, J., Steinman, R. M., Matsuda, Y., and Inaba, K. (2002) Identification and expression of mouse Langerin (CD207) in dendritic cells. *Int. Immunol. 14*, 433–444.
8. Galustian, C., Park, C. G., Chai, W., Kiso, M., Bruening, S. A., Kang, Y. S., Steinman, R. M., and Feizi, T. (2004) High and low affinity carbohydrate ligands revealed for murine SIGN-R1 by carbohydrate array and cell binding approaches, and differing specificities for SIGN-R3 and langerin. *Int. Immunol. 16*, 853–866.
9. Stambach, N. S., and Taylor, M. E. (2003) Characterization of carbohydrate recognition by langerin, a C-type lectin of Langerhans cells. *Glycobiology 13*, 401–410.
10. Kissenpfennig, A., Ait-Yahia, S., Clair-Moninot, V., Stossel, H., Badell, E., Bordat, Y., Pooley, J. L., Lang, T., Prina, E., Coste, I., Gresser, O., Renno, T., Winter, N., Milon, G., Shortman, K., Romani, N., Lebecque, S., Malissen, B., Saeland, S., and Douillard, P. (2005) Disruption of the langerin/CD207 gene abolishes Birbeck granules without a marked loss of Langerhans cell function. *Mol. Cell. Biol. 25*, 88–99.
11. Hunger, R. E., Sieling, P. A., Ochoa, M. T., Sugaya, M., Burdick, A. E., Rea, T. H., Brennan, P. J., Belisle, J. T., Blauvelt, A., Porcelli, S. A., and Modlin, R. L. (2004) Langerhans cells utilize CD1a and langerin to efficiently present nonpeptide antigens to T cells. *J. Clin. Invest. 113*, 701–708.
12. Turville, S. G., Cameron, P. U., Handley, A., Lin, G., Pohlmann, S., Doms, R. W., and Cunningham, A. L. (2002) Diversity of receptors binding HIV on dendritic cell subsets. *Nat. Immunol. 3*, 975–983.
13. Kawamura, T., Kurtz, S. E., Blauvelt, A., and Shimada, S. (2005) The role of Langerhans cells in the sexual transmission of HIV. *J. Dermatol. Sci. 40*, 147–155.
14. de Witte, L., Nabatov, A., Pion, M., Fluitsma, D., de Jong, M. A., de Gruijl, T., Piguet, V., van Kooyk, Y., and Geijtenbeek, T. B. (2007) Langerin is a natural barrier to HIV-1 transmission by Langerhans cells. *Nat. Med. 13*, 367–371.
15. Chatwell, L., Holla, A., Kaufer, B. B., and Skerra, A. (1981) (2008) The carbohydrate recognition domain of Langerin reveals high structural similarity with the one of DC-SIGN but an additional, calcium-independent sugar-binding site. *Mol. Immunol. 45*, 1994.
16. Thépaut, M., Vivès, C., Pompidor, G., Kahn, R., and Fieschi, F. (2008) Overproduction, purification and preliminary crystallographic analysis of the carbohydrate recognition domain of human langerin. *Acta Crystallogr. F 64*, 115–118.
17. Muller, S., Senn, H., Gsell, B., Vetter, W., Baron, C., and Bock, A. (1994) The formation of diselenide bridges in proteins by incorporation of selenocysteine residues: biosynthesis and characterization of (Se)2-thioredoxin. *Biochemistry 33*, 3404–3412.
18. Strub, M. P., Hoh, F., Sanchez, J. F., Strub, J. M., Bock, A., Aumelas, A., and Dumas, C. (2003) Selenomethionine and selenocysteine double labeling strategy for crystallographic phasing. *Structure 11*, 1359–1367.
19. Kabsch, W. (1993) Automatic processing of rotation diffraction data from crystals of initially unknown symmetry and cell constants. *J. Appl. Crystallogr. 26*, 795–800.
20. Collaborative Computational Project, No. (1994) The CCP4 suite: programs for protein crystallography. *Acta Crystallogr. D 50*, 760–763.
21. Vonrhein, C., Blanc, E., Roversi, P., and Bricogne, G. (2006) *Crystallographic Methods*, Humana Press, Totowa, NJ.
22. Emsley, P., and Cowtan, K. (2004) Coot: model-building tools for molecular graphics. *Acta Crystallogr., Sect. D: Biol. Crystallogr. 60*, 2126–2132.
23. Schuck, P. (2000) Size-distribution analysis of macromolecules by sedimentation velocity ultracentrifugation and lamm equation modeling. *Biophys. J. 78*, 1606–1619.
24. Morris, G. M., Goodsell, D. S., Halliday, R. S., Huey, R., Hart, W., Belew, R. K., and Olson, A. J. (1998) Automated docking using a Lamarckian genetic algorithm and and empirical binding free energy function. *J. Comput. Chem. 19*, 1639–1662.
25. Clark, M., Cramer, R. D. I., and van den Opdenbosch, N. (1989) Validation of the general purpose Tripos 5.2 force field. *J. Comput. Chem. 10*, 982–1012.
26. Nurisso, A., Kozmon, S., and Imberty, A. (2008) Comparison of docking methods for carbohydrate binding in calcium-dependent lectins and prediction of the carbohydrate binding mode to sea cucumber lectin CEL-III. *Mol. Simul. 34*, 469–479.
27. Imberty, A., Bettler, E., Karababa, M., Mazeau, K., Petrova, P., and Pérez, S. (1999) in *Perspectives in Structural Biology* (Vijayan, M., Yathindra N., and Kolaskar A. S., Eds.) pp 392−409, Indian Academy of Sciences and Universities Press, Hyderabad.
28. Blundell, T., Carney, D., Gardner, S., Hayes, F., Howlin, B., Hubbard, T., Overington, J., Singh, D. A., Sibanda, B. L., and Sutcliffe, M. (1988) 18th Sir Hans Krebs lecture. Knowledge-based protein modelling and design. *Eur. J. Biochem. 172*, 513–520.
29. Chen, J., Skehel, J. J., and Wiley, D. C. (1999) N- and C-terminal residues combine in the fusion-pH influenza hemagglutinin HA(2) subunit to form an N cap that terminates the triple-stranded coiled coil. *Proc. Natl. Acad. Sci. U.S.A. 96*, 8967–8972.
30. Weis, W. I., and Drickamer, K. (1994) Trimeric structure of a C-type mannose-binding protein. *Structure 2*, 1227–1240.
31. Valladeau, J., Duvert-Frances, V., Pin, J. J., Dezutter-Dambuyant, C., Vincent, C., Massacrier, C., Vincent, J., Yoneda, K., Banchereau, J., Caux, C., Davoust, J., and Saeland, S. (1999) The monoclonal antibody DCGM4 recognizes Langerin, a protein specific of Langerhans cells, and is rapidly internalized from the cell surface. *Eur. J. Immunol. 29*, 2695–2704.
32. Kashihara, M., Ueda, M., Horiguchi, Y., Furukawa, F., Hanaoka, M., and Imamura, S. (1986) A monoclonal antibody specifically reactive to human Langerhans cells. *J. Invest. Dermatol. 87*, 602–607.
33. Laskowski, R. A., MacArthur, M. W., Moss, D. S., and Thornton, J. M. (1993) PROCHECK a program to check the stereochemical quality of protein structures. *J. Appl. Crystallogr. D 26*, 283–291.
34. Balzarini, J. (2007) Targeting the glycans of glycoproteins: a novel paradigm for antiviral therapy. *Nat. Rev. Microbiol. 5*, 583–597.
35. Ng, K. K., Drickamer, K., and Weis, W. I. (1996) Structural analysis of monosaccharide recognition by rat liver mannose-binding protein. *J. Biol. Chem. 271*, 663–674.
36. Ng, K. K., Kolatkar, A. R., Park-Snyder, S., Feinberg, H., Clark, D. A., Drickamer, K., and Weis, W. I. (2002) Orientation of bound ligands in mannose-binding proteins. Implications for multivalent ligand recognition. *J. Biol. Chem. 277*, 16088–16095.
37. Lupas, A., Van Dyke, M., and Stock, J. (1991) Predicting coiled coils from protein sequences. *Science 252*, 1162–1164.
38. Garcia De La Torre, J., Huertas, M. L., and Carrasco, B. (2000) Calculation of hydrodynamic properties of globular proteins from their atomic-level structure. *Biophys. J. 78*, 719–730.
39. Sagebiel, R. W., and Reed, T. H. (1968) Serial reconstruction of the characteristic granule of the Langerhans cell. *J. Cell Biol. 36*, 595–602.
40. Drickamer, K. (1999) C-type lectin-like domains. *Curr. Opin. Struct. Biol. 9*, 585–590.
41. Feinberg, H., Mitchell, D. A., Drickamer, K., and Weis, W. I. (2001) Structural basis for selective recognition of oligosaccharides by DC-SIGN and DC-SIGNR. *Science 294*, 2163–2166.
42. Ward, E. M., Stambach, N. S., Drickamer, K., and Taylor, M. E. (2006) Polymorphisms in human langerin affect stability and sugar binding activity. *J. Biol. Chem. 281*, 15450–15456.
43. Lozach, P. Y., Lortat-Jacob, H., de Lacroix de Lavalette, A., Staropoli, I., Foung, S., Amara, A., Houles, C., Fieschi, F., Schwartz, O., Virelizier, J. L., Arenzana-Seisdedos, F., and Altmeyer, R. (2003) DC-SIGN and L-SIGN are high affinity binding receptors for hepatitis C virus glycoprotein E2. *J. Biol. Chem. 278*, 20358–20366.
44. Navarro-Sanchez, E., Altmeyer, R., Amara, A., Schwartz, O., Fieschi, F., Virelizier, J. L., Arenzana-Seisdedos, F., and Despres, P. (2003) Dendritic-cell-specific ICAM3-grabbing non-integrin is essential for the productive infection of human dendritic cells by mosquito-cell-derived dengue viruses. *EMBO Rep. 4*, 723–728.
45. Alvarez, C. P., Lasala, F., Carrillo, J., Muniz, O., Corbi, A. L., and Delgado, R. (2002) C-type lectins DC-SIGN and L-SIGN mediate cellular entry by Ebola virus in cis and in trans. *J. Virol. 76*, 6841–6844.
46. Geijtenbeek, T. B., Van Vliet, S. J., Koppel, E. A., Sanchez-Hernandez, M., Vandenbroucke-Grauls, C. M., Appelmelk, B., and

Van Kooyk, Y. (2003) Mycobacteria target DC-SIGN to suppress dendritic cell function. *J. Exp. Med. 197*, 7–17.
47. van Die, I., van Vliet, S. J., Nyame, A. K., Cummings, R. D., Bank, C. M., Appelmelk, B., Geijtenbeek, T. B., and van Kooyk, Y. (2003) The dendritic cell-specific C-type lectin DC-SIGN is a receptor for *Schistosoma mansoni* egg antigens and recognizes the glycan antigen Lewis x. *Glycobiology 13*, 471–478.
48. Frison, N., Taylor, M. E., Soilleux, E., Bousser, M. T., Mayer, R., Monsigny, M., Drickamer, K., and Roche, A. C. (2003) Oligolysine-based oligosaccharide clusters: selective recognition and endocytosis by the mannose receptor and dendritic cell-specific intercellular adhesion molecule 3 (ICAM-3)-grabbing nonintegrin. *J. Biol. Chem. 278*, 23922–23929.
49. Tabarani, G., Reina, J. J., Ebel, C., Vives, C., Lortat-Jacob, H., Rojo, J., and Fieschi, F. (2006) Mannose hyperbranched dendritic polymers interact with clustered organization of DC-SIGN and inhibit gp120 binding. *FEBS Lett. 580*, 2402–2408.
50. Borrok, M. J., and Kiessling, L. L. (2007) Non-carbohydrate inhibitors of the lectin DC-SIGN. *J. Am. Chem. Soc. 129*, 12780–12785.
51. Reina, J. J., Sattin, S., Invernizzi, D., Mari, S., Martinez-Prats, L., Tabarani, G., Fieschi, F., Delgado, R., Nieto, P. M., Rojo, J., and Bernardi, A. (2007) 1,2-Mannobioside mimic: Synthesis, DC-SIGN interaction by NMR and docking, and antiviral activity. *ChemMedChem 2*, 1030–1036.
52. Wang, S. K., Liang, P. H., Astronomo, R. D., Hsu, T. L., Hsieh, S. L., Burton, D. R., and Wong, C. H. (2008) Targeting the carbohydrates on HIV-1: Interaction of oligomannose dendrons with human monoclonal antibody 2G12 and DC-SIGN. *Proc. Natl. Acad. Sci. U.S.A. 105*, 3690–3695.
53. Timpano, G., Tabarani, G., Anderluh, M., Invernizzi, D., Vasile, F., Potenza, D., Nieto, P. M., Rojo, J., Fieschi, F., and Bernardi, A. (1921) (2008) Synthesis of novel DC-SIGN ligands with an alpha-fucosylamide anchor. *ChemBioChem 9*, 1930.
54. de Witte, L., Nabatov, A., and Geijtenbeek, T. B. (2008) Distinct roles for DC-SIGN+-dendritic cells and Langerhans cells in HIV-1 transmission. *Trends Mol. Med. 14*, 12–19.
55. Feinberg, H., Castelli, R., Drickamer, K., Seeberger, P. H., and Weis, W. I. (2007) Multiple modes of binding enhance the affinity of DC-SIGN for high mannose N-linked glycans found on viral glycoproteins. *J. Biol. Chem. 282*, 4202–4209.
56. McCaffrey, R. A., Saunders, C., Hensel, M., and Stamatatos, L. (2004) N-linked glycosylation of the V3 loop and the immunologically silent face of gp120 protects human immunodeficiency virus type 1 SF162 from neutralization by anti-gp120 and anti-gp41 antibodies. *J. Virol. 78*, 3279–3295.
57. Scanlan, C. N., Pantophlet, R., Wormald, M. R., Ollmann Saphire, E., Stanfield, R., Wilson, I. A., Katinger, H., Dwek, R. A., Rudd, P. M., and Burton, D. R. (2002) The broadly neutralizing anti-human immunodeficiency virus type 1 antibody 2G12 recognizes a cluster of alpha1→2 mannose residues on the outer face of gp120. *J. Virol. 76*, 7306–7321.
58. Hanau, D., Fabre, M., Schmitt, D. A., Stampf, J. L., Garaud, J. C., Bieber, T., Grosshans, E., Benezra, C., and Cazenave, J. P. (1987) Human epidermal Langerhans cells internalize by receptor-mediated endocytosis T6 (CD1 "NA1/34") surface antigen. Birbeck granules are involved in the intracellular traffic of the T6 antigen. *J. Invest. Dermatol. 89*, 172–177.
59. Bartosik, J. (1992) Cytomembrane-derived Birbeck granules transport horseradish peroxidase to the endosomal compartment in the human Langerhans cells. *J. Invest. Dermatol. 99*, 53–58.
60. Andersson, L., Bartosik, J., Bendsoe, N., Malmström, A., Mikulowska, A., Warfvinge, K., Andersson, A., and Falk, B. (1988) in *The Langerhans Cell* (Thivolet, J., and Schmitt, D., Eds.) pp 185−191.
61. Verdijk, P., Dijkman, R., Plasmeijer, E. I., Mulder, A. A., Zoutman, W. H., Mieke Mommaas, A., and Tensen, C. P. (2005) A lack of Birbeck granules in Langerhans cells is associated with a naturally occurring point mutation in the human Langerin gene. *J. Invest. Dermatol. 124*, 714–717.
62. Mommaas, M., Mulder, A., Vermeer, B. J., and Koning, F. (1994) Functional human epidermal Langerhans cells that lack Birbeck granules. *J. Invest. Dermatol. 103*, 807–810.
63. Kleijmeer, M. J., Oorschot, V. M., and Geuze, H. J. (1994) Human resident langerhans cells display a lysosomal compartment enriched in MHC class II. *J. Invest. Dermatol. 103*, 516–523.
64. Mc Dermott, R., Ziylan, U., Spehner, D., Bausinger, H., Lipsker, D., Mommaas, M., Cazenave, J. P., Raposo, G., Goud, B., de la Salle, H., Salamero, J., and Hanau, D. (2002) Birbeck granules are subdomains of endosomal recycling compartment in human epidermal Langerhans cells, which form where Langerin accumulates. *Mol. Biol. Cell 13*, 317–335.
65. McMahon, H. T., and Gallop, J. L. (2005) Membrane curvature and mechanisms of dynamic cell membrane remodelling. *Nature 438*, 590–596.

BI802151W